

A Study on the Channel and Gap Flow Simulation for Electrical Discharge Micro-Drilling of Inconel 718 Superalloy

Magdalena Machno^{1*}, Marcin Trajer², Adrian Czeszkiewicz², Paulina Żurawka³

¹ Department of Rail Vehicles and Transport, Faculty of Mechanical Engineering, Cracow University of Technology, al. Jana Pawła II 37, 31-864 Cracow, Poland

² General Electric Aerospace Poland, al. Krakowska 110/114, 02-256 Warsaw, Poland

³ Łukasiewicz Research Network – Institute of Aviation, al. Krakowska 110/114, 02-256 Warsaw, Poland

* Corresponding author's e-mail: magdalena.machno@pk.edu.pl

ABSTRACT

The process of electrical discharge micro-drilling (micro-EDD) of micro holes is used in the aviation, automotive and biomedical industries. In this process, an important issue affecting the stability and efficiency of the process is the flow of the working fluid through the tool electrode channel and the front and side gap areas. Because tool electrodes have diameters below 1 mm. Many factors present in the EDM-drilling process occurring on a micro scale mean that a full explanation of the phenomena affecting the process is limited. The solution is to analyze the phenomena in the process based on the results of numerical simulations, which are based on real measurements. The aim of this work is to analyze the flow of de-ionized water through a brass single-channel electrode with a channel diameter of 0.11 mm and a front and side gap. The liquid flow was analyzed for various variants (with and without cavitation, with added rotation of the tool electrode, with and without surface roughness with material particles). In simulation, it is important to gradually increase the complexity of the model, starting with the simplest model and gradually adding further phenomena. Analysis of the simulation results showed a significant impact on the liquid flow of cavitation, as well as the presence of vortex gaps in some areas, which have a significant impact on the process of drilling micro holes.

Keywords: electrical discharge micro-drilling (micro-EDD), micro-hole, fluid flow via micro-channel, numerical simulation.

INTRODUCTION

The Electrical Discharge Machining (EDM) process has been known almost a hundred years. This manufacturing technique is utilized mostly for materials that are difficult to machine via conventional methods. Among the materials for which the EDM process is used, there are innovative engineering materials, such as nickel-chromium superalloys, titanium alloys, permanently hardened, very hard materials [1–3]. Strength and thermal parameters of such alloys or superalloys allow for their use for parts in aviation and automotive industries [4,5]. Furthermore, many parts in these industries require micro-scale geometries, for example, the manufacturing technology

of turbine blades in aviation. Using EDM, micro-holes are drilled in the turbine blades. The number of such micro-holes per part is usually several hundred and 18–30,000 in a combustion chamber [6,7]. The micro-holes (with diameters less than 1 mm) are often deep, with the ratio of depth to diameter of up to 600:1. The amount and geometry of the micro-holes shows how efficient their manufacturing method should be. Currently, the most commonly used process in such cases is Electrical Discharge Machining [8,9].

However, EDM also has its limitations, which creates huge challenges for the manufacturing process [10]. It still needs an improvement in efficiency and a reduction in the tool electrode consumption [11]. The limitations of the technique

also include the accuracy of the micro-hole geometry and their quality. The phenomena occurring throughout the EDM process still require more research. Additionally, new alloys and superalloys are still being developed for the aviation and automotive industries, and their thermal properties (such as low thermal conductivity, high melting temperature) influence the process of material removal via EDM [4,12].

In the process of the EDM micro-hole drilling, some of the occurring phenomena still need to be researched further and reduced due to their detrimental impact on process efficiency. Among them, one can name the accumulation of the eroded material particles at the bottom area of the hole, the extensive use of the tool electrode (in case of micro-machining – even up to 100%), efficient flushing of the machining area (front gap, side gap) [13–15]. The last factor has a significant impact on the efficiency of the micro-hole drilling process [16].

The research on the flow through the machining area in the EDM process is still being conducted [17]. According to [14], the flow of a dielectric liquid through the electrode channel and the area of the side and front gap is significant for the micro-EDD process. Studies on the liquid flow through the electrode dedicate a single channel electrode to create deep micro-holes. In case of micro-drilling, multi-channel electrodes seem to be less effective [18]. It is worth noting that the flow of the liquid influences the stability of the process as well as its efficiency and tool electrode consumption [19]. In [20], it is analyzed the significance of the dielectric liquid flow in the EDM process. The results of their studies show that the flow strongly influences the removal mechanism. The intensity of the flow impacts the front topography of the hole. Up to 15 l/h, one could observe certain erosion craters on the machined surface, however, for higher flow intensities it is nearly impossible to identify such craters. Moreover, it is assumed that the reduction in electrode consumption is an effect of better cooling of the machining area for higher flow intensities, as the heat produced during the discharge and causing the consumption is removed faster at higher intensities. In [21], the conclusions from the analysis based on experimental testing and from a numerical simulation also confirm the significant impact of the dielectric flow velocity on the EDD process. The depth of the whole, flushing velocity, and the tool diameter all influence the gap flow area and debris distribution. The increase of hole depth leads to a decrease in liquid

frequency in the bottom gap, which hinders the debris removal. At the same time, the increase in liquid flushing velocity removes more debris from the bottom of the interelectrode gap. Higher diameters for the liquid flow are beneficial for lowering the resistance in removing the liquid and debris. However, when the depth of the machined hole reaches a certain degree (depth-to-diameter ratio exceeds 3), the influence of the flushing velocity and tool diameter on the debris removal is visibly decreased, which leads to a considerable amount of debris at the bottom.

Due to the size of the machining area (front and side gaps) in the order of 10–100 μm , it is helpful to conduct an analysis of the machining flow conditions in the EDD process using numerical simulations. Studies analyze various phenomena and aspects regarding the flow of the machining liquid flow through the interelectrode gap. In [22], a numerical model was studied to quantitatively determine the heat transfer between the machined object and the flushing flow in a typical EDM hole. It was concluded that the debris particles have a significant impact on the heat flux through the machined object. In a different study [23], the flow velocity distribution in the interelectrode gap was analyzed for various depth-to-diameter ratios, taking into account the change in geometry of the tool electrode tip. The data in the simulation was defined based on experimental tests. The analysis of the results showed that as the depth-to-diameter ratio increases, the flow velocity of the working liquid in the gap decreases, which makes debris removal more difficult. Also, the effect of flushing the working liquid on the particles in the machining gap decreases with the increase of the depth-to-diameter ratio, which leads to incorrect discharges. Moreover, it was proven that as the depth-to-diameter ratio increases, the axial wear of the electrode increases. Simulations of working fluid flushing through the interelectrode gap including the material particles have also been analyzed in [21]. The analysis discovered an accumulation of a considerable amount of debris in the hole bottom area. Flushing velocity is crucial for debris removal from the machining area. In this work, it is emphasized that for deep holes with diameters below 1 mm, the working liquid flows through the interelectrode gap slower. Slower flow may lead to insufficient removal of eroded material particles, which may cause secondary discharges. Also, the accumulation

of debris at the bottom of the hole may increase conductivity of the dielectric fluid. The analysis of holes with depths over 5 mm showed the presence of burk marks, which confirms excessive electrical discharges in that area. The simulation also proved that for the hole depth of 5 mm, almost all the debris remained at the bottom.

The literature study above proves that the phenomena such as liquid flow through the interelectrode gap and the accumulation of eroded particles related to it should still be analyzed. In accordance with above information, it is worth it to analyze the phenomenon of a dielectric liquid flow through an electrode with a diameter of less than 1 mm. A crucial aspect of the flow analysis might be including each phenomenon present throughout the process step by step.

The article is focused on the flow of de-ionized water through a brass single-channel electrode with a channel diameter 0.11 mm and through the side and front gaps. The analysis is based on a flow simulation in Ansys Fluent. The simulation was prepared based on the previously conducted studies of the flow of de-ionized water through a single-channel electrode with 0.3 mm outer diameter and 0.11 mm inner channel diameter. The flow was analyzed for various cases, such as: flow including cavitation, the impact of electrode rotation, impact of surface roughness of the inner channel and the hole area, impact of material particle presence in the interelectrode gap. The main goal of the simulation was to investigate the impact of aforementioned phenomena on the micro-EDD process. For that reason, the complexity of the simulation was increased step by step, analyzing the flow with and without the mentioned processes.

The analysis of the results of such de-ionized water flow simulation will allow for better understanding of phenomena occurring in the side and front gaps throughout the micro-EDD process. Moreover, the gradual increase in complexity and separating each phenomenon will allow to investigate their impact more thoroughly. As an effect, the results of the analysis may help in further optimization of the micro-EDD process in order to increase its efficiency (material removal rate – MRR, hole geometry accuracy) and reduce the tool electrode consumption.

Tool electrode wear in the EDM process is an important factor, but the simulation analysis focuses on analyzing the impact on the liquid flow through the electrode channel and the gaps (front

and side). In particular, the influence of factors such as cavitation effect, electrode rotation speed, roughness of the electrode surface and the hole surface, and the presence of particles in the inter-electrode space, are also analyzed.

MATERIALS AND METHODS

First, experimental tests of liquid flow through a brass single-channel electrode were performed. The choice of this type of electrode resulted from its use for electro-erosion drilling of micro-holes. According to [18], single-channel electrodes provide the best results in the micro-EDD process. De-ionized water at a temperature of 293.15 K was used as the dielectric fluid. Then, the test data were used to develop a model and simulate the liquid flow through the electrode channel and the front and side gap area in the hole.

To test the flow of the working fluid, a single-channel brass electrode with an outer diameter of $\varnothing 0.3$ mm and a channel diameter of $\varnothing 0.11$ mm was selected (Figure 1). The calculated area of the electrode channel is 0.019 mm^2 and constitutes the flow area of the working liquid. Since the working electrode is worn out in the EDM process, an electrode with a nominal length of 400 mm (nominal tool electrode) and an electrode shortened by 64%, with a length of 145 mm (shorter tool electrode) were selected for experimental flow tests. In this way, the influence of working electrode wear was taken into account in the research [23]. Moreover, it was important to obtain test results that would enable the creation of a simulation reflecting the actual drilling process as much as possible.

For both electrodes (nominal length and shorter), 10 repetitions of water flow through the channel were performed. A single flow test lasted 1 min. Flow was measured using a mini-CORI FLOW™ M14 micro flowmeter (The Netherlands, Bronkhorts®). The measurement was made automatically every 0.1 seconds and with the mass flow accuracy better than $\pm 0.2\%$ Rd. The liquid was supplied to the electrode channel under appropriate, automatically controlled pressure. The aim of this research was to check and analyze the water flow through the electrode channel, and the results were used to define the simulation. The diagram below schematically illustrates the measurement of liquid flow through the electrode channel (Figure 2).

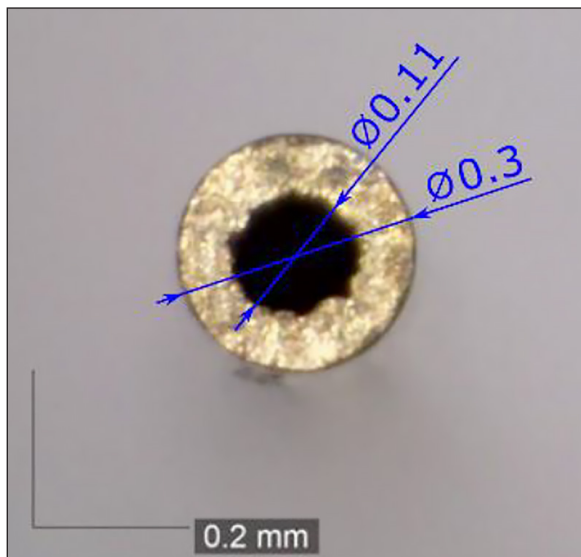


Figure 1. Tool electrode tip face

The efficiency and stability of liquid flow through the electrode channel are influenced by the geometry of the electrode (especially the geometry of the tip of the electrode face) and the quality of the electrode channel (its diameter along the entire length of the electrode and surface roughness). Electrodes often differ in quality of workmanship, even though they come from the same manufacturer and the same batch. Used electrodes in the tests purchased from Transcorn Sp. z o.o. Therefore, it was decided to check the quality and dimensional and shape accuracy of the electrodes used. To check the dimensional accuracy of the electrode, spatial scanning of the tip of the new electrode and the channel inside the electrode (Figure 3) was performed using the Alicona C200 microscope system (Alicona Imaging

GmbH, Raaba/Graz, Austria). In order to measure the channel geometry, it was necessary to gain access to the inside of the channel. For this purpose, the electrode was embedded in resin and then its side wall was polished on a laboratory polisher. The measurement of the diameter of the channel inside the electrode was repeated three times in selected places. The average canal diameter calculated from the measurements was 0.11 mm. The surface roughness of the channel wall was also measured. The average value of the channel surface roughness Ra was $12\ \mu\text{m}$. The roughness of the outer wall of the electrode was also measured – $Ra = 9.5\ \mu\text{m}$, and the roughness of the wall of the workpiece – $Ra = 3.3\ \mu\text{m}$. Surface roughness measurements were also made using the Alicona apparatus.

In order to show how the quality of electrode production in EDM-drilling affects the flow of working liquid through the channel, photos were taken of the liquid flow through the channel of a correctly made and defective electrode (Figure 4). The correct speed of liquid flow through the channel ensures proper process efficiency and maintaining stable process conditions.

Disturbances in the flow of liquid through the channel most often occur due to the poorer quality of the channel surface. This is due to the lack of guidelines for the quality of manufactured electrodes. It happens that electrodes from the same batch have different manufacturing quality. Most often, better quality of electrodes and its repeatability for the entire batch is determined by the higher price of the electrodes. In the photo below, you can see how significant the difference is in the flow of liquid through the channel with proper

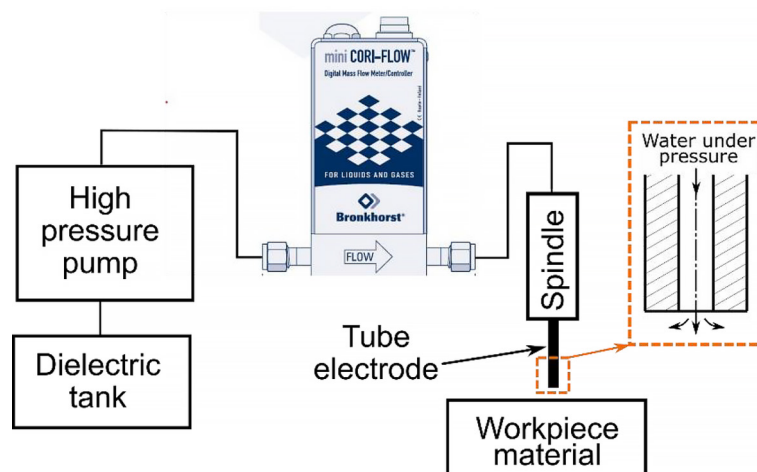


Figure 2. Application of micro mass flow meter

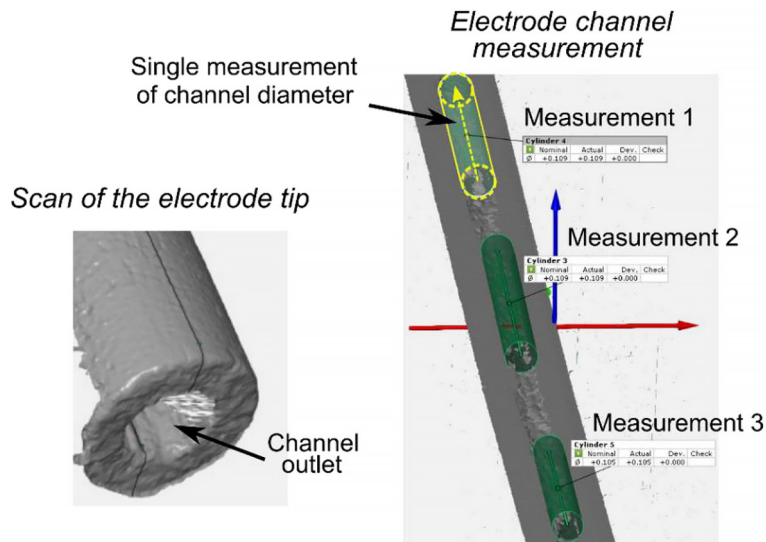


Figure 3. Method of measuring the geometry of a tool electrode

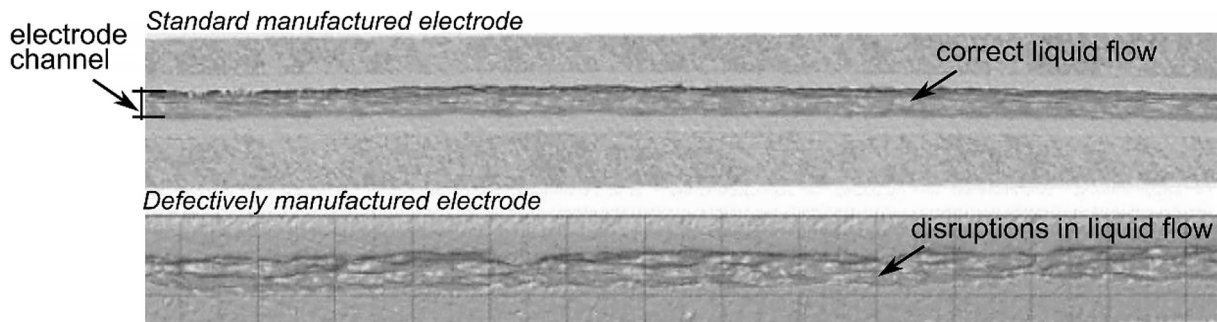


Figure 4. Comparison of liquid flow through the channel of a properly made and defective electrode

surface roughness and worse. Due to the observed discrepancies in the quality of the electrodes, the liquid flow rate through a new electrode should be checked each time before starting the EDM drilling process. This lengthens the overall process, and technological time is a very important factor in the industry.

Electrical discharge drilling is used to make micro-holes in parts of turbine blades in the aviation industry. The blades are made of modern engineering materials, most often nickel-chromium superalloys. Therefore, the machined material used for turbine blades was selected for the simulation: Inconel 718, a nickel-chromium superalloy. Also, the selected electrode material - brass,

is dedicated to Inconel 718 machining [24]. Table 1 shows the measured chemical composition of the workpiece material and tool electrode material. The chemical composition was measured using an X-MET8000 X-ray spectrometer (Hitachi High-Tech, Tokyo, Japan).

In the electroerosion process, the thermo-physical properties of the workpiece material and the tool electrode material are important due to the thermal energy present in the EDM process. Table 2 shows selected properties of the Inconel 718 superalloy and brass. Selecting the appropriate tool electrode material affects the process efficiency and its stability. To confirm the selection of the appropriate material for the tool electrode,

Table 1. Chemical composition of Inconel 718 and brass electrode (%)

Inconel 718											Brass	
Ni	Cr	Fe	Nb	Mo	Ti	Al	Co	Si	Cu	W	Cu	Zn
56.63	18.40	16.81	5.37	3.16	0.96	0.57	0.1	0.34	0.08	0.06	68.67	31.33

Table 2. Thermophysical properties of the analyzed materials

Property (unit)	Inconel 718 [25,26]	Brass [27,28]
Density (g/cm ³)	8.19	8.55
Melting point (K)	1,533–1,609	1,263
Thermal conductivity (W/(m K))	11.4	159
Specific heat capacity (J/(kg K))	435	385

the erosion resistance index (ER_{index}) was calculated – based on, for brass and Inconel 718. This index shows the fit of the tool electrode material to the machined material. Based on this indicator, it is also assessed how well the material is processed by the electroerosion process. The following, Equation 1 shows how to calculate the erosion resistance index [29].

$$ER_{index} = \lambda \cdot c \cdot T^2 \quad (1)$$

where: λ – thermal conductivity (W/(m K)), c – specific heat capacity (J/(kg K)), T – melting point (K). The values of λ , c , T were taken from Table 2 (in the case of a range of values, the maximum value in the range was considered).

The formula describing ER_{index} indicates that the melting point of the material has the most significant impact on the machinability of the material by EDM – the value of the melting point is squared. The calculated ERindex for Inconel 718 was 1.28, and for brass it was 9.76. According to the interpretation of the ER_{index} in case when value of this index for workpiece material is higher than its value for tool electrode material, this indicates that electrode material is correct. Moreover, the calculated ER_{index} of the workpiece material is much larger than that of the electrode material, indicating the good EDM machinability of the Inconel 718 superalloy by the brass electrode.

Since the work analyzes the flow of dielectric liquid through the electrode channel and the processing area, Table 3 presents the selected properties of de-ionized water at a temperature of 293.15 K.

The main aim of this work is to investigate the flow of deionized water through the tool electrode channel and the area of the front gap and side gap. For this purpose, it was decided to analyze the results with different flow variants adopted. Moreover, the complexity of the simulation was increased stepwise to make it possible to observe the greatest possible impact of individual phenomena on the liquid flow. The analyzed

variants and phenomena defined in the simulation are listed below:

- liquid flow with the electrode located above the surface of the processed material and with the electrode immersed to a certain depth in the hole,
- simulation of flow with and without cavitation,
- influence of electrode rotation on liquid flow,
- the influence of the surface roughness of the tool electrode and the workpiece material,
- the influence of the presence of material particles in the interelectrode space.

RESULTS – THE DE-IONIZED WATER FLOW THROUGH THE ELECTRODE CHANNEL

First, the water flow through the channel of the nominal electrode and the shorter electrode was analyzed. For the nominal electrode, an initially higher flow of approximately 465 g/min was observed, followed by a decrease to approximately 13 g/min (Figure 5). The further water flow through the channel is maintained at a level of approximately 13 g/min. In this case, the higher flow rate value at the beginning of the measurement resulted from the valve opening. Then the water flow rate stabilizes to a constant value, correct for an electrode with a diameter of 0.3 mm.

However, for the shorter electrode, a lower flow rate value of approximately 15 g/min is observed at the beginning, and then its increase to a

Table 3. Selected properties of the de-ionized water at a temperature of 293.15 K during saturation pressure

Physical properties	Value
Density, (kg/m ³)	998.2
Specific heat, (kJ/(kg K))	4.183
Thermal conductivity, (W/(m K))	0.6
Kinematic viscosity, (m ² /s)	1.06 · 10 ⁶
Electrical conductivity, (μS/cm)	0.04194
Resistivity, (MΩcm)	23.844

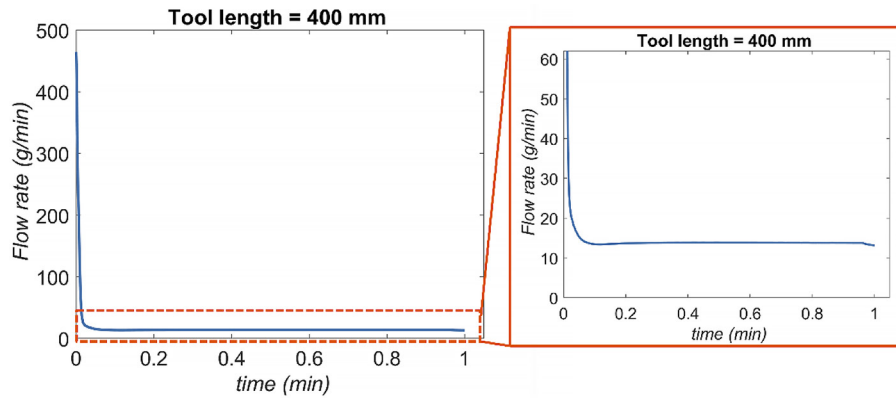


Figure 5. Measured flow rate for the nominal electrode

stable value of approximately 20.8 g/min (Figure 6). The higher stable value compared to the stable flow rate value for the nominal electrode results from the liquid flow over a shorter distance (145 mm). This is a natural phenomenon for liquid flow. Because the difference between the flow rate for the nominal electrode and the shortened electrode is not large (approx. 5 g/min). It was decided that the average value of the flow velocity from the tests (16 g/min) would be used in the simulation. Moreover, for this reason, the impact of electrode wear on flow conditions was not analyzed in the simulation. The work focused on the analysis of other factors (mentioned earlier). However, in further research, the impact of shortening the working electrode on the liquid flow should be examined more thoroughly.

Since the flow rate of the liquid is different for the nominal electrode and the shorter electrode, the Reynolds number (Re) was calculated based on formula 2. The Reynolds number gives

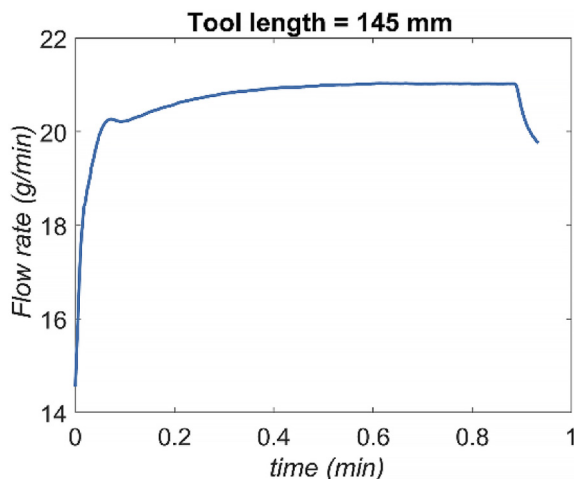


Figure 6. Measured flow rate for the shorter electrode

information about the nature of the liquid flow through the channel - laminar or turbulent [14].

$$Re = (v \cdot r) / \gamma \quad (2)$$

where: r – the radius of the channel diameter in the tool electrode, γ – the kinematic viscosity of the working fluid ($\gamma = 1.06 \cdot 10^{-6} \text{ m}^2/\text{s}$ for de-ionized water at 293.15 K), v – flow rate velocity. The flow rate velocity of the fluid was calculated from the following formula 3:

$$v = Q / F \text{ (m/s)} \quad (3)$$

where: Q – liquid flow rate (m^3/s) – assumed stable values, F is a cross-section area of the electrode’s channel (m^2). The electrode channel area is $9.5 \cdot 10^{-9} \text{ m}^2$, and the calculated values of the flow rate velocity were 24.4 m/s for the nominal electrode and 36.5 m/s for the shorter electrode, respectively.

The calculated Reynolds number for the liquid flow through the nominal electrode and the shorter electrode was 1332 and 1994, respectively. Until the Reynolds number is below 2300, laminar flow is assumed, and above this value the flow is turbulent [14]. However, the analyzed liquid flow is for an electrode (tube) with a flow diameter of 0.11 mm. As indicated in the work [30] the limit of the laminar-turbulent transition in microchannels occurs at Reynolds numbers much lower than at the macro scale. In the work of G.M. Mala, D.Li estimated that in the considered microchannels the transition to turbulence begins at Reynolds numbers $Re > 300-900$. Also Wang and Peng (1994) [31] indicate in their research results that for micro-channels with diameters in the range of 0.2–0.8 mm, the transition from laminar to turbulent flow occurred when Re

< 800, and that fully developed turbulent Convection was initiated in the Reynolds number range of 1000–1500. For the calculated Reynolds numbers, it was decided to assume turbulent flow in the simulation.

RESULTS – MODELLING PROCEDURE

In order to reduce the size of the model while striving to reflect real phenomena, it was decided to divide the analysis into two separate models. The first model (Model 1, Figure 7) concerns the flow of liquid through a free electrode placed above the surface of the workpiece at a distance of 30 μm. This distance was also the thickness of the front gap. This model made it possible to match the numerical model to the results from real measurements. However, the second model

(Model 2, Figure 7) concerns an electrode immersed in the hole at a depth 0.3 mm and 1.00 mm. For the model of the electrode immersed in the hole, the energy equation was included in the calculation and the turbulence model was chosen to be SST k-omega. The temperature on both inlet and outlet was set to 293.15 K, as was measured. In this model, a side gap thickness of 50 μm is additionally defined. The distances between the electrode and the material - the front gap thickness and the side gap thickness - were imposed arbitrarily based on the process settings used. All simulations were conducted for stationary models after achieving steady-state.

For a clear analysis of the simulation results, Figure 8 explains the defined electrode geometry and hole geometry in Ansys with reference to the diagrams in Figure 7. Model 1 illustrates the conditions at the beginning of the drilling process, where

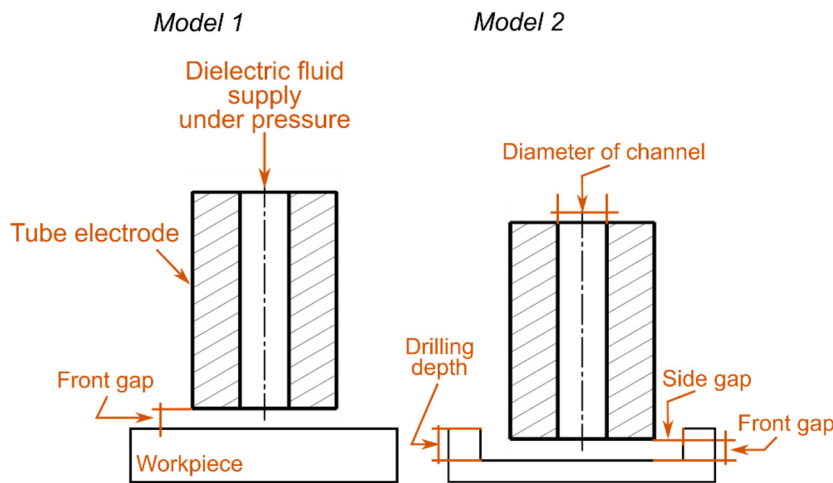


Figure 7. Schemes of the analyzed models used in the simulation

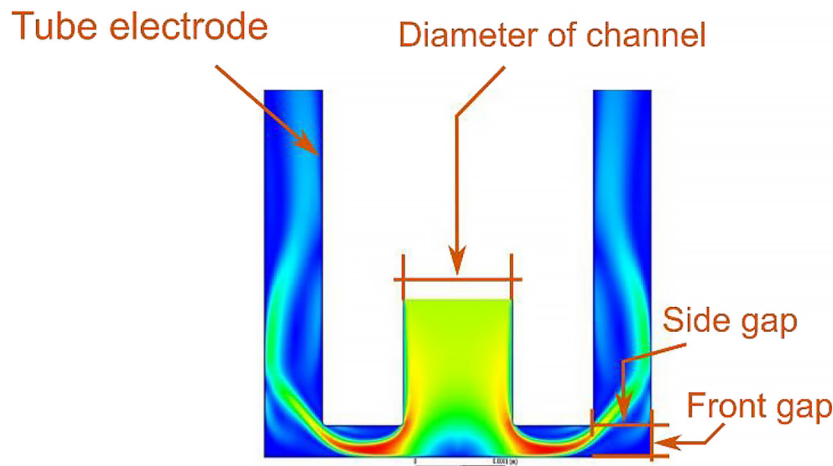


Figure 8. Electrode geometry and hole geometry in the Ansys Fluent program

the electrode is still some distance from the surface of the workpiece. However, model 2 illustrates the conditions during drilling at selected two hole depths. Both cases considered (free electrode and immersed in the hole) were modeled in Ansys® 2020 R2. However, in order to cover the created geometry with a finite volume mesh, two programs were used – ICEM for a free electrode and Ansys Meshing for an electrode embedded in a hole. The complexity of the simulation was increased step by step, starting with the simplest model and gradually adding further phenomena to be able to trace their impact on the flow process as far as possible.

First, model 1 was developed, which is a two-dimensional (2D) axisymmetric model. The ICEM mesh created for the free electrode model is a simple mesh with inflation applied in order to capture boundary layer effects close to the wall. The mesh quality was verified to fulfill the requirements posed by the chosen turbulence model (k-epsilon), e.g. the y^+ parameter. In this model, the electrode geometry was defined and then a mesh was applied to it (Figure 9). The electrode geometry was defined based on scanning data and measurements of the nominal electrode. This allowed us to obtain the electrode dimensions necessary to create the model - the internal and external diameters of the electrode. The quality of the mesh and its volume were checked. Because if the mesh density is too low or the elements are too deformed, the results could be unreliable. It turned out that the selected type of mesh volume had no impact on the results. For this model, atmospheric pressure was set as the boundary conditions as water pressure at the inlet and outlet of the electrode channel. The prepared model was

loaded into the Ansys Fluent program, where the specifications regarding physical phenomena were specified. Because the flow through the electrode can be classified as incompressible, the Solver type was set to ‘Pressure-based’. To account for all possible effects acting on the electrode, gravity was also included. For this purpose, the value of 9.81 m/s^2 was assumed in the program for ‘Gravitational Acceleration’.

An important element influencing the flow of liquid through the channel is the quality of the channel surface. For this purpose, the channel surface roughness was defined in the program. Using the measured roughness values Ra , the parameter Ks (equivalent sand-grain roughness height) was defined, which is the numerical equivalent of the surface roughness coefficient Ra in the Fluent program [32, 33]. The values from roughness measurements were scaled to obtain the appropriate value of the Ks parameter. The Ks parameter was controlled to obtain compliance in the flow between the actual measurement and the numerical model. For the coefficient value $Ks = 5.54 \cdot 10^{-6} \text{ m}$, the results were consistent. A roughness constant (Cs) of 0.5 was also adopted, which is the value defined for turbulent flow.

However, in model 2, the mass flow determined from measurements was used at the electrode inlet and atmospheric pressure at the electrode outlet. Similarly to the model for the free electrode, the model assumed axial symmetry of the problem with pressure boundary conditions and a flat model. After establishing the basic geometric assumptions (Table 4), the correctness of the mesh was verified (Figure 10). A model with a basic hybrid mesh with the option to scale the

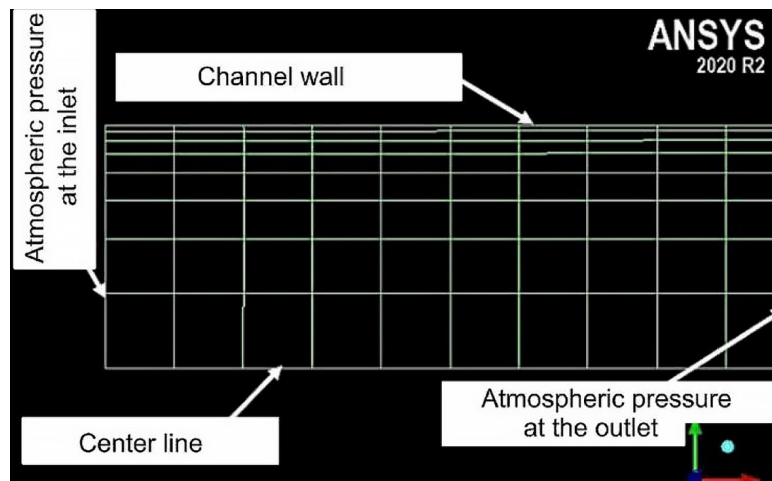


Figure 9. The 2D free electrode model

Table 4. Parameters to define the mesh grid

Value	Element quality	Orthogonal quality	Skewness
Maximum	1	1	0.48
Minimum	0.557	0.72	1.3e-10
Average	0.9	0.9978	3.63e-003

element size and a model with a simple mesh with inflation were developed. Cavitation was also analyzed phenomenon in the model. Cavitation was defined in the program using the multiphase ‘Mixture’ model with settings for cavitation.

During the EDM drilling process, the tool electrode rotates. This element was also included in this model. For this purpose, the ‘axisymmetric swirl’ setting was turned on and the angular velocity of the electrode walls was set to 500 rpm. Using the literature [10], it was assumed that the impact of turnover should be small. Finally, the model was supplemented with a simulation of solid particles, which are the equivalent of the material removed during processing. The behavior of material particles detached from both the surface of the processed material and the electrode tip was analyzed. For this purpose, the ‘Discrete Phase Modeling’ function was used, where particles were set to be released from the above surfaces. The ‘Rosin-Rammler logarithmic’ setting was used for their size distribution, and the appropriate material type was also assigned (nickel-chromium superalloy and brass).

DISCUSSION

Firstly, a simulation was conducted to verify the velocity distribution for the flow through the electrode channel with applied surface roughness of the channel walls. The analysis of the results shows that at first the flow is non-homogeneous, however, the turbulence profile stabilizes rather fast and is homogeneous throughout the majority of the electrode (Figure 11). With a constant intensity of the volumetric flow, the pressure gradient required to push the liquid through the micro-tube is higher than expected based on conventional theory. Moreover, the impact of the micro-tube material and surface roughness of the channel is a factor here.

The complexity of the model was increased gradually. This approach would allow to analyze the impact of each separate phenomenon more accurately. The first step was to include the energetic relations. At this stage, the walls of both the hole and the electrodes were modeled as perfectly smooth, without applying surface roughness parameters. For that case, the velocity and static pressure distributions were analyzed for the electrode modelled inside the hole (Figure 12). This allowed to verify the created grids. The differences in results were 0.82% for velocity and 2% for maximum pressure, which allowed to use the primary mesh as well defined.

For the velocity distribution, an increase in flow velocity can be observed at the exit of the electrode channel into the front gap. In this area, the liquid under certain pressure moves into an area with dimensions smaller than the channel diameter (0.05 mm vs 0.11 mm). As expected for a fluid flow in such conditions: the velocity is increased when it flows in from a wider to a narrower area. For verification, the water velocity v for the higher and lower surface areas was calculated based on the formula (3). It was assumed that the flow intensity is 16 g/min, as in the simulation, and the flow area was calculated as the product of the front gap thickness and the difference between the electrode diameter and channel

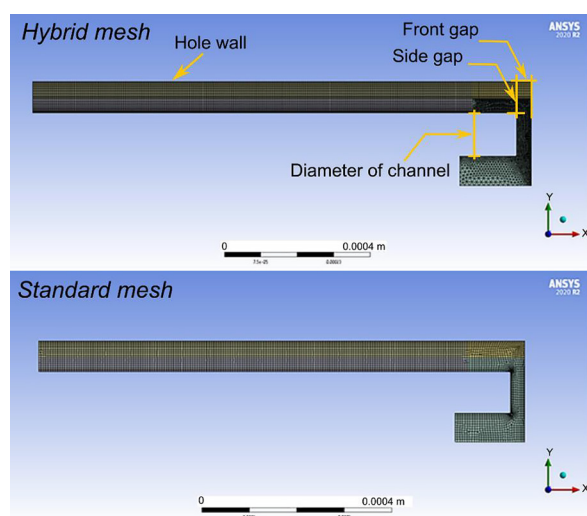


Figure 10. Hybrid mesh – basic hybrid mesh with the option of scaling element sizes and standard model – simple mesh with inflation

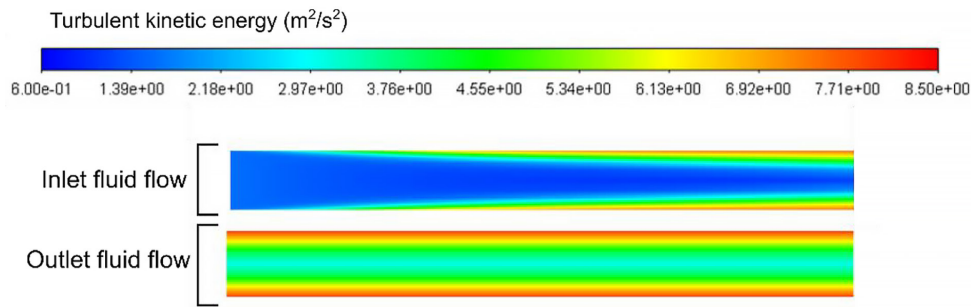


Figure 11. Distribution of turbulent kinetic energy at the electrode inlet (top profile) and at the outlet (bottom profile)

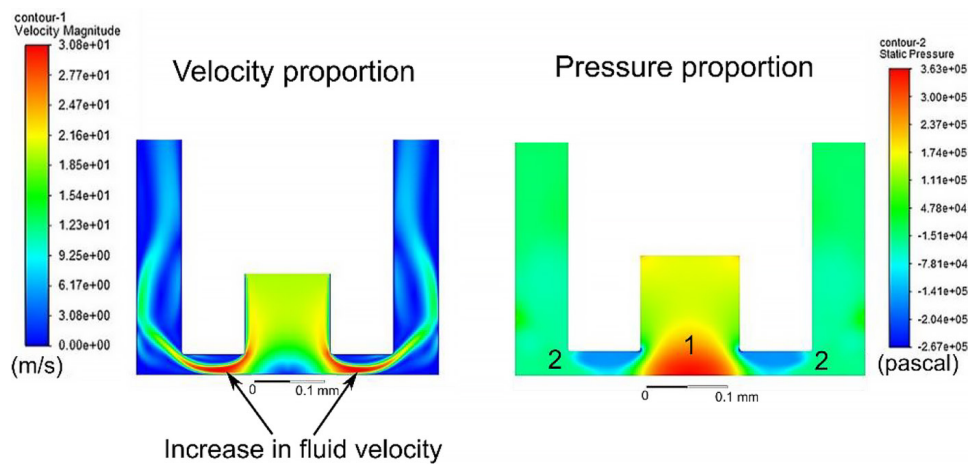


Figure 12. Cross-sections with the distribution of velocity and static pressure

diameter. The obtained value of the flow through the channel was 28 m/s, and 56 m/s through the front gap. Additionally, the area of the electrode tip ring creates a certain resistance to the flow through the front gap. Based on the calculations and simulation results, the increase in flow velocity in the front gap area after it leaves the electrode channel is the correct phenomenon [20].

For the pressure distribution, one can observe an increase in pressure after the liquid comes in contact with the surface of the hole bottom (area no. 1 in Figure 12). It is the correct behavior for a liquid under pressure after it meets a flat surface. When the liquid is under pressure, it acts on a given surface with a normal pressure force. Then, as it leaves the front gap, its pressure drops (area no. 2 in Figure 12).

The next step in the simulation was to enable cavitation to verify its influence on the fluid flow. To present the effect, multi-phase flow was enabled. This helped to locate areas where water evaporates due to a significant pressure drop. Knowing that allowed to analyze whether

cavitation has an influence on the front and side gap flow. In Figure 13 below, one can observe that cavitation does significantly affect the flow – at least at the early phase of the electrode running, while its tip remains close to the nominal geometry. In the marked areas – at the edges of the electrode channel, cavitation can be observed.

Moreover, in Figure 14, the liquid flow was compared with and without the cavitation setting. The results show vortices forming in the gap area. The presence of these vortices in such areas can also be seen in [22].

Comparing the two cases, clear differences in the vortices can be seen. Also, the streamline itself is also different in each case. For the simulation that includes cavitation, vortices form on both sides of the water streamline. Based on simulation and experimental results on EDM micro-holes, the cavitation model better resembles real conditions of the process. For the cavitation case, the streamline skips past the edge of the electrode tip and stays in contact with a larger area of the bottom of the hole. The vortices also form at the

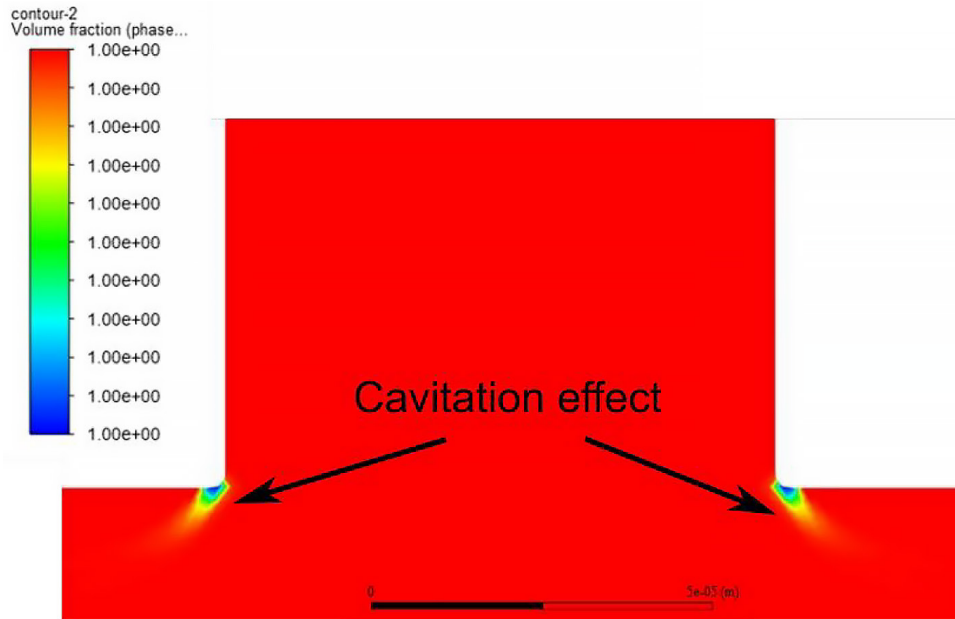


Figure 13. Electrode channel with visible corners where water cavitation occurs

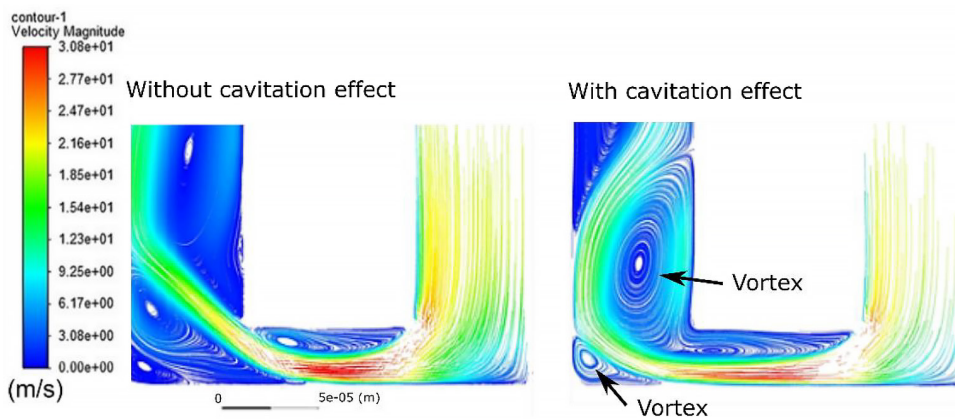


Figure 14. Streamlines for the interelectrode gap area without and with the cavitation phenomenon taken into account

electrode wall, which is not observed in the simulation without cavitation

In the real process, the particles of eroded material can be found at the machining area. The debris moving along with the rotating liquid may also be the reason for excessive electrical discharges (so called secondary/abnormal discharges). In such case, the extra discharges may occur between the debris and the outer surface of the electrode. Secondary discharges also results in wear of the electrodes, mainly on the side wall at the tip [34]. Analyzing the simulation results, the areas of vortex occurrence are close to the side wall of the electrode at its tip and in the corner of the hole. It is in these areas that excessive material removal is observed (electrode needling and

excessively enlarged hole diameter) [35]. Taking into account the phenomenon of accumulation of debris in the area of the inter-electrode gap, the presence of vortices makes it difficult for debris to escape from the hole. Therefore, it can be concluded that the formed vortices also influence the occurrence of secondary discharges and, at the same time, the above-mentioned deformations in the geometry of the hole and electrode.

The influence of the tool electrode rotation on the fluid flow was also verified. The rotational velocity was taken to be 500 rpm. The simulation results for the model without surface roughness (Figure 15) showed that the swirl velocity distribution is negligible. Similar results were obtained [34 36]. In the real EDM process, when the deep

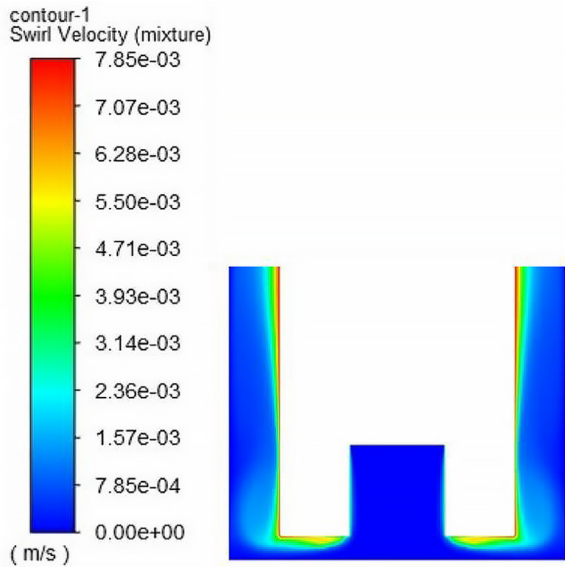


Figure 15. Model with added tool electrode rotation

micro-hole is performed, the electrode rotation helps maintain a stable drilling process and improves its efficiency. However, the experimental results from a real EDM process also show that the influence of the tool electrode rotation is comparably smaller than the influence of electrical parameters of the process (working voltage, current intensity amplitude, impulse time length). Here, the simulation results confirm the lesser impact of tool electrode rotation on the liquid flow in the machining area.

On a surface machined using EDM, erosion craters occur, which influence the surface quality [38]. The excessive electrical discharges in the bottom area of the hole further worsen the surface roughness. The next step in the simulation was to include the previously calibrated surface roughness of the hole and electrode channel. This factor has the greatest impact on the flow through the electrode channel [30]. Here, the results from

the first model of the free electrode were used. Adding a coefficient simulating the actual surface roughness to the model showed that the quality of the surface significantly influences the results (Figure 16). It is also an important conclusion regarding the production of electrodes and the quality of the surface in the channel. Electrode manufacturers should provide information on the surface roughness of the electrode channel.

The extra friction caused by the flow resistance at the walls caused the liquid to ‘stick’ to the hole walls on one hand, and an increase in its velocity on the other. Incorporating the roughness caused the streamline to ‘stick’ to the hole wall across a larger area. For a model without defined roughness, the maximum flow velocity was 12 m/s. For the model including the surface roughness friction, the velocity was 30 m/s. This means that the liquid accumulates its energy at the walls, which could be expected. This shows how crucial the surface quality is in the EDD process, both for the electrode channel and the hole walls. The influence of the surface roughness in the flow through the electrode channel is also studied in [30]. For the quality of the hole walls, it is defined throughout the process and depends in large on applied process parameters. However, the quality of the channel surface can be controlled at the electrode production stage. Information about surface roughness of the channel inside the electrode should be given by the electrode producer. Moreover, the value of the surface roughness of the channel should lie within specified tolerances. Electrodes that do not fulfill this requirement should not be sold.

Next, the simulation was used to verify the flow for different electrode setups, such as: at the workpiece surface (Figure 17a), submerged to 0.3 mm hole depth, and to 1 mm hole depth (Figure 17b).

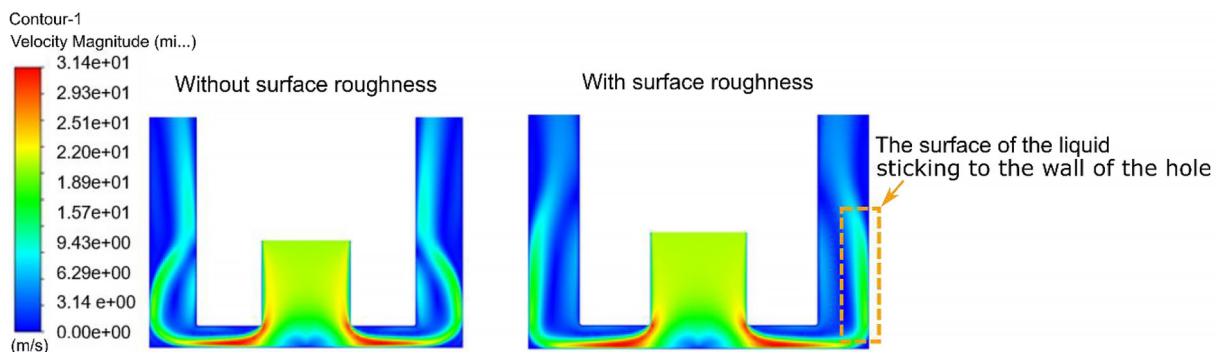


Figure 16. The influence of roughness on the flow near the electrode tip

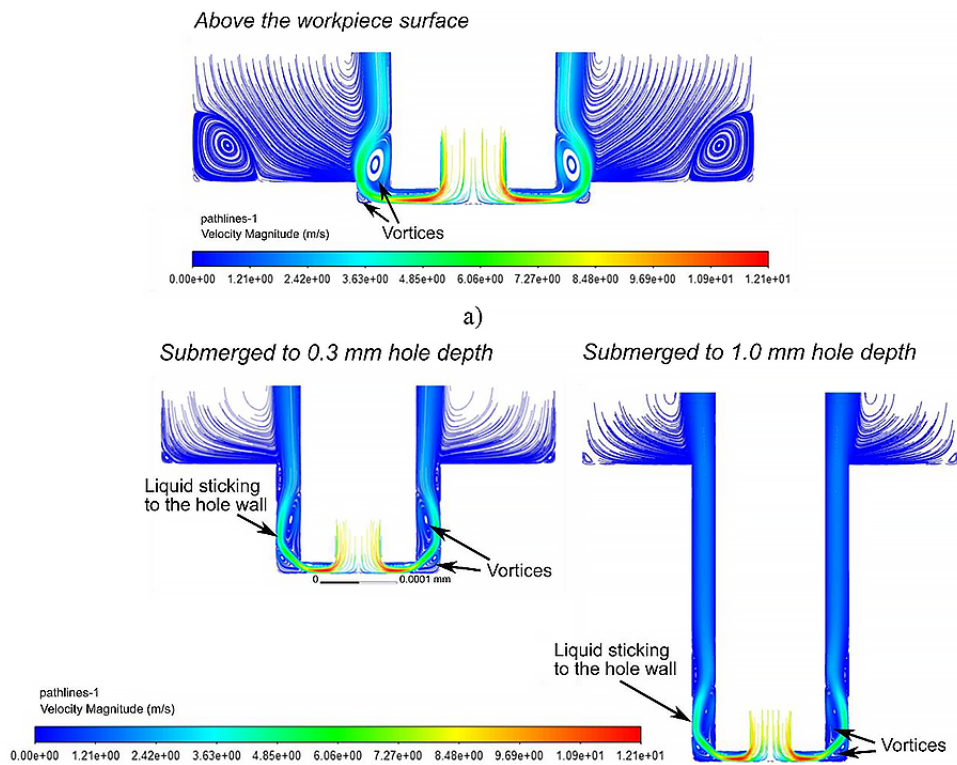


Figure 17. Liquid flow for different position of the tool electrode, (a) at the height of the workpiece surface, (b) in the hole at a depth of 0.3 mm and of 1 mm

For all analyzed cases, the nature of the liquid flow is similar. The water stream flowing out of the channel into the front slot has a higher speed. Then, the liquid flows through the face gap at this higher speed. Then, after reaching the side gap, the speed of the water stream is lower. When water flows outside the hole, the water stream bypasses the corner of the hole. This shows that this area of the hole is not being flushed. This would explain the accumulation of material particles in this area. And as is known from other works [37], the accumulation of particles of eroded material at the bottom of the hole favors the formation of secondary discharges. Secondary discharges enhance material removal at the bottom of the hole and also contribute to excessive electrode wear on the sidewall (so called needling). Similar simulation results in the well day area were obtained in [34, 35]. It is also worth emphasizing that with the increasing depth of the hole (during drilling), the surface roughness of the hole wall increases [39]. In work [40] it also is concluded that debris removal problems usually occur during deep operations. The increase in the surface roughness of the hole wall at its bottom probably also affects the velocity of the liquid as it escapes from the hole. In this work, the influence of changing surface

roughness along the length of the hole was not analyzed. However, this factor certainly requires investigation in further research and simulations.

It is worth to notice the vortices formed. Their presence confirms the turbulent flow of the liquid, which is characterized by swirl occurrence. The swirl phenomenon may explain difficulties in full removal of the erosion products from the hole bottom. The debris along with the rotating liquid does not flow towards the exit of the hole but stays within. The debris, while near the hole wall or the side wall of the electrode, is facing conditions contributing to so called secondary electrical discharges. Both the tool electrode and the machined material are connected to an electrical impulse generator at all times, which makes such discharges possible. As an effect, the material at the bottom of the hole is being additionally removed, which leads to an increased output diameter and needling at the tip of the tool electrode. The currently existing technological solutions are to use specifically adjusted non-conducting coating on the outer wall of the electrode, or to change the electrode tip shape. It is worth mentioning that these solutions do get rid of the secondary discharge occurrences, but the debris at the bottom of the hole still accumulates. That is why efficient flow through these areas seems to be

a crucial matter. Moreover, the technology of applying such isolating coating on the side surface for an electrode with the diameter of less than 1 mm is a demanding and costly process, similarly as changing the geometry of the tip of the electrode.

As shown by the results from [41], as the depth of the hole increases, MRR decreases due to deteriorated evacuating condition of debris particles. As the phenomenon of the eroded material particle accumulation within the interelectrode gap is still being studied, it was verified in the simulation. To check for the presence of debris in the machining area, the Ansys Discrete Phase Model- Particle Tracking module was used. The distribution of particle size was as described by Tanjilul in [16]. In Figure 18, one can see the material particles released during the simulation.

Assuming the nominal geometry leads to a very sharp corner at the bottom of the hole, where the particles gather – which can be explained by the physics of the flow. The streamline, when

faced with a perpendicular wall, must change direction – the particles it carries are then ‘thrown out’ into the corner of the hole. Such accumulation can be seen in the Figure 18. In the side gap area, the particle distribution is homogenous and is included in the range of $0-1.92e^{-11}$ kg of particles per m^3 of fluid.

In order to better understand the flow through the gaps and the movement of the particles, another analysis was run with a narrowed scale (Figure 19). In the simulation results, two kinds of particle movement can be identified. They can be divided into movement of particles along the streamline – marked by 1 in Figure 19 – and movement of particles along the forming vortices – marked by 2 in Figure 19. The movement lines corresponding to the vortices are dominating in the results of the simulations, there is more of them than those along the streamline. This explains why a significant amount of particles remains in the side gap, and some of them accumulate at the bottom of

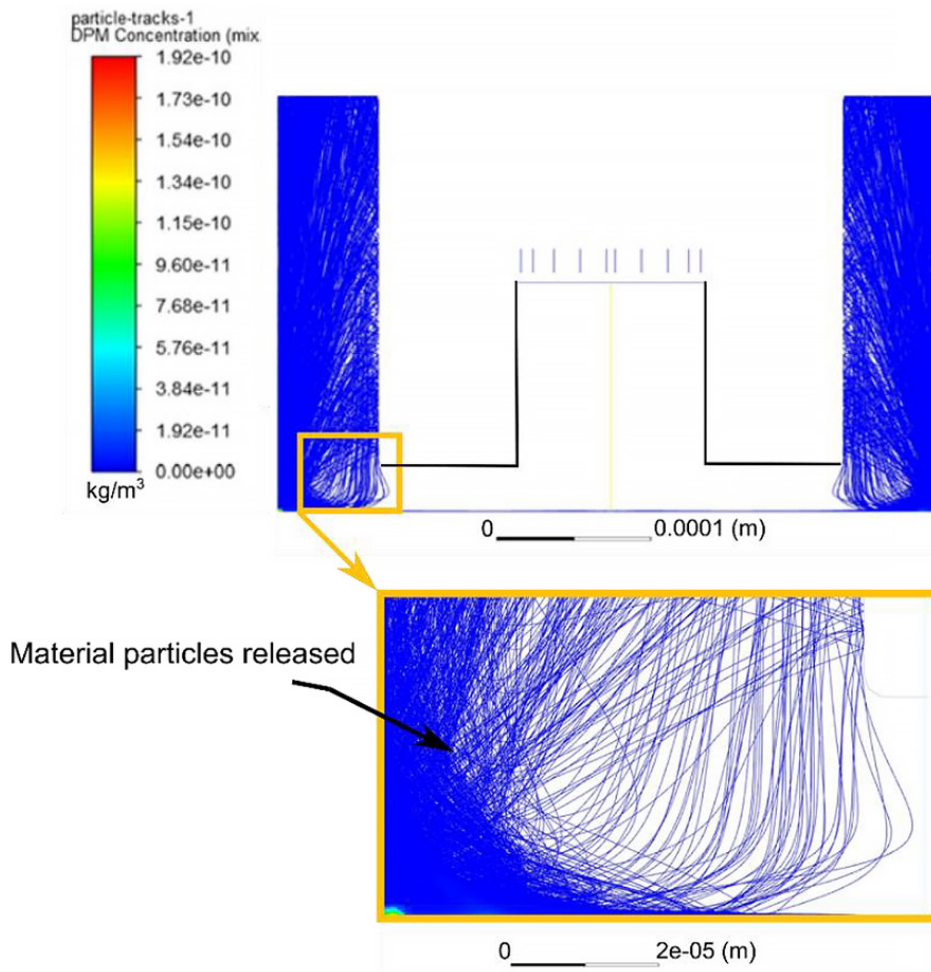


Figure 18. Particles released from the material in full view with a close-up of the particles accumulated in the corner of the bottom of the hole

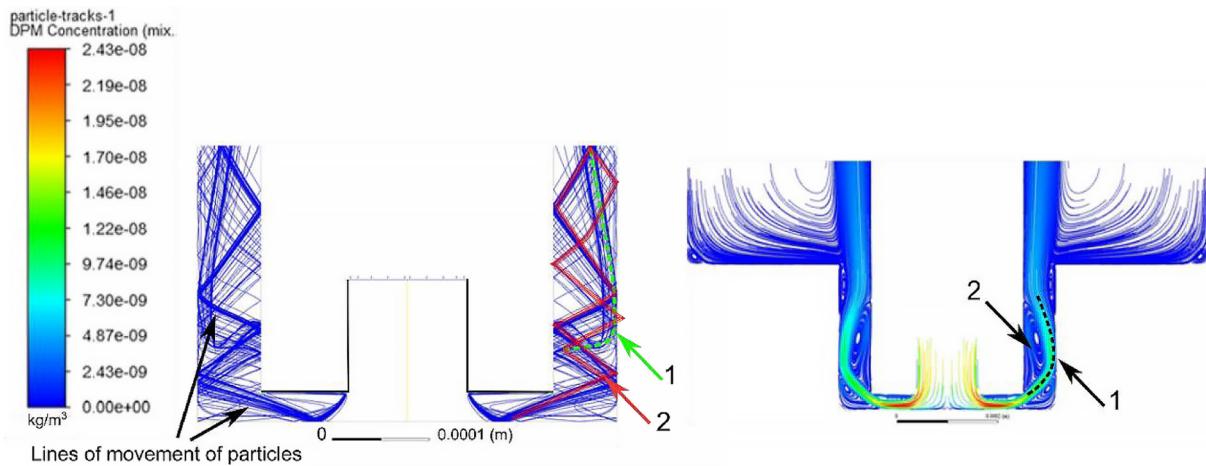


Figure 19. View with a narrowed scale to show the lines of movement of particles in the front gap and side gap areas

Table 5. Summary of the impact of the analyzed factors on the flow

Analyzed factor influencing the flow	The importance of influence
Cavitation effect	High
Tool electrode rotation	Small
Roughness surface	High
Hole depth	Medium

the hole. The results of the simulation also strongly confirm the turbulence of the flow with its existence of vortices. The phenomena observed at this stage of the simulation show that if the swirl presence is high in the real process, removing eroded pieces of material from the hole will be a challenge in the EDD process. Considering the size of the front gap and the side gap as well as the influence of the liquid flow, efficient flushing is a critical aspect.

In earlier analyses, the corners at the bottom of the whole were defined as sharp. However, during the process, the corner gets rounded due to the excessive material removal in that area. It was therefore investigated how those material particles would distribute for a rounded corner (Figure 18). The rounded corner and the influence of the wall roughness lead to particles starting to accumulate along the wall. We can therefore conclude that the change in the hole bottom geometry is also an important factor that needs to be considered.

Eliminating the sharp corner not only changes the bottom geometry, but also the maximal values of static pressure and velocity. For a hole with perpendicular corners, the maximal velocity of the flow is 30.9 m/s, and for the rounded corner model it is 31.4 m/s. This change may stem

from the reduced cross-section area around the side gap (especially at the exit from front gap to side gap) by the debris accumulated on the hole wall. In case of static pressure, the increase in its value for the rounded model is from 4.35×10^5 Pa to 4.54×10^5 Pa. Analyzing all these changes, one can notice that they are relatively small. However, in the case of a simulation, where all values and factors are defined, they cannot be ascribed to any other additional factor (as can happen for the real process). This means that the hole bottom geometry has a significant impact on the change in flow velocity. Knowing the results from an actual EDD process, one can observe rounding at the bottom of the whole and a greater output diameter.

Additionally, the Table 5 summarizes the influence of the analyzed factors on the flow of the working liquid through the electrode channel and the gaps (front and side). It was determined how strongly these factors affect the flow: high, medium, small.

CONCLUSIONS

In this work, the liquid flow through the electrode channel and the areas of the front gap and side gap were analyzed. The analysis was carried out based on a developed simulation using the Ansys Fluent program. Based on the analysis of the results, the most important conclusions are formulated below:

- the phenomenon of cavitation should be taken into account in simulation of the flow of liquids. The results of simulation shows that the cavitation effect has a high important influence on the liquid flow,

- the surface roughness inside the hole turned out to be a factor that strongly influenced the nature of the liquid flow through the slots (front and side). The simulation showed that the defined surface roughness causes a larger surface of the water stream to stick to the walls of the hole,
- the simulation results showed the formation of vortices in the area close to the electrode wall and in the corner of the hole, which is also confirmed by simulations by other researchers. The presence of vortices confirms the turbulent movement of the liquid flow. It can also be assumed that the vortices that form in the area of the inter-electrode gap contribute to the deformation of the hole geometry and wear of the electrode on the side wall,
- the simulation results confirm the lesser impact of tool electrode rotation on the flow liquid through channel and the gaps.

Analysis of the simulation results showed that it is worth checking the fluid flow for defined different hole surface roughnesses at different hole depths. In actual results, the surface roughness increases with the hole depth. It would be worth examining how the flow changes at different depths of the hole with changing surface roughness. Assuming that the defined surface roughness should be increased in increasingly deeper areas of the hole.

Since the analysis of the simulation results showed that the surface roughness of the electrode channel affects the liquid flow rate, the channel surface roughness parameter should be provided by the electrode manufacturers.

REFERENCES

1. Arshad R., Mehmood S., Shah M., Imran M., Qayyum F. Effect of distilled water and kerosene as dielectrics on machining rate and surface morphology of Al-6061 during electric discharge machining. *Advances in Science and Technology Research Journal*. 2019; 13(3): 162–169.
2. Santarao K, Prasad C, Swami Naidu G. Experimental investigation to study the viscosity and dispersion of conductive and non-conductive nanopowders' blended dielectrics. *Advances in Science and Technology Research Journal*. 2017; 11(1): 154–160.
3. Struzikiewicz, G. Investigation of the cutting fluid incidence angle direction in turning grade 5 ELI titanium alloy under high-pressure cooling conditions. *Materials*. 2023; 16(15): 5371.
4. Trajer M., Czeszkiewicz A., Machno M. Analysis of the relationship between the properties of selected materials and the parameters of the EDD process. In: *Material Forming: The 26th International ES-AFORM Conference on Material Forming held in Kraków, Poland 2023 April 19–21, 1747–1758*.
5. Lipiec P., Machno M., Skoczypiec S. The experimental research on electrodischarge drilling of high aspect ratio holes in Inconel 718. In: *AIP Conference Proceedings, Palermo, Italy 2018 April 23–25, 1960(1)*.
6. Yuri M.T., Masada J., Tsukagoshi K., Ito E., Hada S. Development of 1600 °C-class high-efficiency gas turbine for power generation applying J-type technology. *Mitsubishi Heavy Industries Technical Review*. 2013; 50(3): 1–10.
7. Klocke F., Klink A., Veselovac D., Aspinwall D.K., Leung Soo S., Schmidt M., Schilp J., Levy G., Kruth J.-P. Turbomachinery component manufacture by application of electrochemical, electro-physical and photonic processes. *CIRP Annals*. 2014; 63(2): 703–726.
8. Li G., Natsu W., Yu Z. Study on quantitative estimation of bubble behavior in micro hole drilling with EDM. *International Journal of Machine Tools and Manufacture*. 2019; 146(103437).
9. Kliuev M., Boccadoro M., Perez R., Dal Bó W., Stirnimann J., Kuster F., Wegener K. EDM drilling and shaping of cooling holes in Inconel 718 turbine blades. *Procedia CIRP*. 2016; 42: 322–327.
10. Machno M., Trajer M., Bizoń W., Czeszkiewicz A. A Study on accuracy of micro-holes drilled in Ti-6Al-4V alloy by using electrical discharge machining Process. *Advances in Science and Technology Research Journal*. 2022; 16(6): 55–72.
11. Arshad R., Mehmood S., Shah M., Imran M., Qayyum F. Effect of distilled water and kerosene as dielectrics on machining rate and surface morphology of Al-6061 during electric discharge machining. *Advances in Science and Technology Research Journal*. 2019; 13(3): 162–169.
12. Maccarini G., Pellegrini G., Ravasio Ch. Effects of the properties of workpiece, electrode and dielectric fluid in micro-EDM drilling process. *Procedia Manufacturing*. 2020; 51: 834–841.
13. Ekmekci B., Sayar A. Debris and consequences in micro electric discharge machining of micro-holes. *International Journal of Machine Tools and Manufacture*. 2013; 65: 58–67.
14. Kliuev M., Baumgart C., Wegener K. Fluid dynamics in electrode flushing channel and electrode-workpiece gap during EDM drilling. *Procedia CIRP*. 2018; 68: 254–259.
15. Machno M., Matras A., Szkoda M. Modelling and analysis of the effect of EDM-drilling parameters on the machining performance of Inconel 718 using the RSM and ANNs methods *Materials*. 2022; 15(3): 1152.

16. Tanjilul M., Ahmed A., Senthil Kumar A., Rahman M. A study on EDM debris particle size and flushing mechanism for efficient debris removal in EDM-drilling of Inconel 718. *Journal of Materials Processing Technology*. 2018; 255: 263–274.
17. Brito Gadeschi G., Schneider S., Mohammadnejad M., Meinke M., Klink, W. Schröder A., Klocke F. Numerical analysis of flushing-induced thermal cooling including debris transport in electrical discharge machining (EDM). *Procedia CIRP*. 2017; 58: 116–121.
18. Kliuev M., Baumgart C., Büttner H., Wegener K. Flushing velocity observations and analysis during EDM drilling. *Procedia CIRP*. 2018; 77: 590–593.
19. Liang W., Tong H., Li B., Li Y. Feasibility research on break-out detection using audio signal in drilling film cooling holes by EDM. *Procedia CIRP*. 2020; 95: 566–571.
20. Munz M., Risto M., Haas R. Specifics of flushing in electrical discharge drilling. *Procedia CIRP*. 2013; 6: 83–88.
21. Zhang Z., Zhang W., Liu Y., Ma F., Su Ch., Sha Z. Study on the gap flow simulation in EDM small hole machining with Ti alloy. *Advances in Materials Science and Engineering*. 2017; 2017: 1–23.
22. Brito Gadeschi G., Schilden T., Albers M., Vorspohl J., Meinke M., Schröder W. Direct particle–fluid simulation of flushing flow in electrical discharge machining. *Engineering Applications of Computational Fluid Mechanics*. 2021; 15(1): 328–343.
23. Liu H., Bai J. The tool electrode wear and gap fluid field simulation analysis in micro-EDM drilling of micro-hole array. *Procedia CIRP*. 2020; 95: 220–225.
24. Kuppan, P., Narayanan, S., Oyyaravelu, R., Balan, A.S.S. Performance evaluation of electrode materials in electric discharge deep hole drilling of Inconel 718 superalloy. *Procedia Engineering*. 2017; 174: 53–59.
25. Pan Z., Feng Y., Hung T.P., Jiang Y.C., Hsu F.C., Wu L.T., Lin C.F., Lu Y.C., Liang S.Y. Heat affected zone in the laser-assisted milling of Inconel 718. *Journal of Manufacturing Processes*. 2017; 30: 141–147.
26. Hernández M., Amriz R.R., Cortès R., Gómora C.M., Plascencia G., Jaramillo D. Assessment of gas tungsten arc welding thermal cycles on Inconel 718 alloy. *Transactions of Nonferrous Metals Society of China*. 2019; 29: 579–587.
27. Khan A.A. Electrode wear and material removal rate during EDM of aluminum and mild steel using copper and brass electrodes. *The International Journal of Advanced Manufacturing Technology*. 2008; 39: 482–487.
28. Suhardjono. Characteristics of electrode materials on machining performance of tool steel SKD11 with EDM shinking. *ARNP: Journal of Engineering and Applied Sciences*. 2016; 11: 986–991.
29. Reynaerts D., Heeren P.-H.'s, van Brussel H. Microstructuring of silicon by electro-discharge machining (EDM)-part I: theory. *Sensors and Actuators A: Physical*. 1997; 60(1–3): 212–218.
30. Mohiuddin Mala Gh., Li D. Flow characteristics of water in microtubes. *International Journal of Heat and Fluid Flow*. 1999; 20(2): 142–148.
31. Wang B.W., Peng X.F. Experimental investigation on forced flow convection of liquid flow through microchannels. *International Journal of Heat and Mass Transfer*. 1994; 37(1): 73–82.
32. Mullya S.A., Karthikeyan G. CFD simulation of dielectric fluid flow in micro electro discharge milling process. *Materials Today: Proceedings*. 2018; 5(11): 24792–24798.
33. Adams T., Grant Ch. A simple algorithm to relate measured surface roughness to equivalent sand-grain roughness. *International Journal of Mechanical Engineering and Mechatronics*. 2012; 1(1): 66–71.
34. Murray J.W., Sun J., Patil D.V., Wood T.A., Clare A.T. Physical and electrical characteristics of EDM debris. *Journal of Materials Processing Technology*. 2016; 229: 54–60.
35. Ferraris E., Castiglioni V., Ceysens F., Annoni M., Lauwers B., Reynaerts D. EDM drilling of ultra-high aspect ratio micro holes with insulated tools. *CIRP Annals*. 2013; 62(1): 191–194.
36. Ahmed A., Boban J., Rahman M. Novel EDM deep hole drilling strategy using tubular electrode with orifice. *CIRP Annals*. 2021; 70(1): 151–154.
37. Murray J., Zdebski D., Clare A.T. Workpiece debris deposition on tool electrodes and secondary discharge phenomena in micro-EDM. *Journal of Materials Processing Technology*. 2012; 212(7): 1537–1547.
38. Thirumalai Kumaran S., Ko T.J., Uthayakumar M. et al. Surface texturing by dimple formation in TiAl-SiZr alloy using μ -EDM. *Journal of the Australian Ceramic Society*, 2017; 53: 821–828.
39. Machno M., Bogucki R., Szkoda M., Bizoń W. Impact of the deionized water on making high aspect ratio holes in the Inconel 718 alloy with the use of electrical discharge drilling. *Materials*. 2020; 13(6): 1476.
40. Zhang W., Liu Y., Zhang S., Ma F., Wang P., Yan Ch. Research on the Gap Flow Simulation of Debris Removal Process for Small Hole EDM Machining with Ti Alloy. *Proc. of the 4th International Conference on Mechatronics, Materials, Chemistry and Computer Engineering*, Held, China 2015, 2121–2126.
41. Wang Y.Q., Cao M.R., Yang S.Q., Li W.H. Numerical simulation of liquid-solid two-phase flow field in discharge gap of high-speed small hole EDM drilling. *Advanced Materials Research* 2008; 53–54: 409–414.